1   **Assessing snow extent data sets over North America to inform and improve trace gas**

2   **retrievals from solar backscatter**

3   Matthew J. Cooper[1], Randall V. Martin[1,2], Alexei I. Lyapustin[3], and Chris A. McLinden[4]

4   1. Department of Physics and Atmospheric Science, Dalhousie University, Halifax, Nova Scotia,

5   Canada.

6   2. Harvard-Smithsonian Center for Astrophysics, Cambridge, Massachusetts, USA

7   3. NASA Goddard Space Flight Center, Greenbelt, MD, USA

8   4. Air Quality Research Division, Environment and Climate Change Canada, Toronto, Ontario,

9   Canada

10   **Abstract**

11   Accurate representation of surface reflectivity is essential to tropospheric trace gas retrievals

12   from solar backscatter observations. Surface snow cover presents a significant challenge due to

13   its variability and thus snow-covered scenes are often omitted from retrieval data sets; however,

14   the high reflectance of snow is potentially advantageous for trace gas retrievals. We first

15   examine the implications of surface snow on retrievals from the upcoming TEMPO

16   geostationary instrument for North America. We use a radiative transfer model to examine how

17   an increase in surface reflectivity due to snow cover changes the sensitivity of satellite retrievals

18   to NO_2 in the lower troposphere. We find that a substantial fraction (>50%) of the TEMPO field

19   of regard can be snow covered in January, and that the average sensitivity to the tropospheric

20   NO_2 column substantially increases (doubles) when the surface is snow covered.

21   We then evaluate seven existing satellite-derived or reanalysis snow extent products against

22   ground station observations over North America to assess their capability of informing surface

23   conditions for TEMPO retrievals. The Interactive Multisensor Snow and Ice Mapping System

24   (IMS) had the best agreement with ground observations (accuracy of 93%, precision of 87%,

25   recall of 83%). Multiangle Implementation of Atmospheric Correction (MAIAC) retrievals of

26   MODIS-observed radiances had high precision (90% for Aqua and Terra), but underestimated

27   the presence of snow (recall of 74% for Aqua, 75% for Terra). MAIAC generally outperforms

28   the standard MODIS products (precision of 51%, recall of 43% for Aqua; precision of 69%,

recall of 45% for Terra). The Near-real-time Ice and Snow Extent (NISE) product had good precision (83%) but missed a significant number of snow-covered pixels (recall of 45%). The Canadian Meteorological Centre (CMC) Daily Snow Depth Analysis Data set had strong performance metrics (accuracy of 91%, precision of 79%, recall of 82%). We use the F score, which balances precision and recall, to determine overall product performance (F = 85%, 82(82)%, 81%, 58%, 46(54)% for IMS, MAIAC Aqua(Terra), CMC, NISE, MODIS Aqua(Terra) respectively) for providing snow cover information for TEMPO retrievals from solar backscatter observations. We find that using IMS to identify snow cover and enable inclusion of snow-covered scenes in clear-sky conditions across North America in January can increase both the number of observations by a factor of 2.1 and the average sensitivity to the tropospheric NO_2 column by a factor of 2.7.

1. Introduction

Satellite observations of solar backscatter are widely used as a source of information on atmospheric trace gases (Richter and Wagner, 2011). These observations have provided valuable information on vertical column densities of O_3, NO_2, SO_2, CO, HCHO, CH_4 and other important trace gases in the troposphere (Fishman et al., 2008). Satellite observations of trace gases have been used to assess air quality (Duncan et al., 2014; Martin, 2008) and to gain insight into atmospheric processes including emissions (Streets et al., 2013), lifetimes (Beirle et al., 2011; Fioletov et al., 2015; de Foy et al., 2015; Valin et al., 2013), and deposition (Geddes and Martin, 2017; Nowlan et al., 2014). The utility of these observations is dependent on their quality, and thus ensuring retrieval accuracy is essential.

Previous studies have found that retrieved NO_2 vertical column densities are highly sensitive to errors in assumed surface reflectance (Boersma et al., 2004; Lamsal et al., 2017; Martin et al., 2002). Much of this error sensitivity results from observation sensitivity to trace gases in the lower troposphere. The observation sensitivity is accounted for in the air mass factor (AMF) conversion of observed line-of-sight "slant columns" to vertical column densities. Uncertainties in surface reflectance are a significant contributor to AMF uncertainty.

57   Existing reflectivity climatologies (e.g. Kleipool et al., 2008; Koelemeijer et al., 2003;

58   Liang et al., 2002; Herman and Celarier, 1997) do not represent snow cover well, since the

59   statistical methods to exclude reflective clouds from the climatologies also exclude variable

60   snow cover; Correspondingly, surface snow may be mistaken for cloud, leading to errors in

61   cloud fraction and pressure estimates used in trace gas retrievals (Lin et al., 2015; O'Byrne et al.,

62   2010; Vasilkov et al., 2017). Therefore, snow cover is particularly challenging to retrievals.

63   Misrepresenting surface snow cover can lead to large errors (20-50%) in retrieved NO_2 columns

64   over broad regions with seasonal snow cover (O'Byrne et al., 2010). For this reason,

65   observations over snow are often omitted or flagged as unreliable to avoid potential errors. This

66   limits the ability of satellite retrieved data sets to offer adequate temporal and spatial sampling in

67   winter months. Additionally, over highly reflective surfaces such as snow observation sensitivity

68   to the lower troposphere is larger and has less dependence on *a priori* NO_2 profiles (Lorente et

69   al., 2017; O'Byrne et al., 2010); Thus, omitting snow-covered scenes means omitting the

70   observations with the greatest sensitivity to the lower troposphere. This could be remedied by

71   using a product that would allow for snow cover identification to be done with confidence.

72   Several data products provide information on snow extent using surface station

73   observations, satellite-observed radiances, or visible imagery. Previous evaluations have found it

74   difficult to determine which of these products is definitively the best, partly due to differences in

75   resolution. Most products are more consistent during the winter months when persistent, deep

76   snow is present (Frei et al., 2012; Frei and Lee, 2010). However, disagreements are common

77   during accumulation and melting seasons, over mountains, and under forest canopies. These

78   evaluations have largely focused on local or regional snow cover or have included only cloud-

79   free observations.

80   The upcoming geostationary Tropospheric Emissions: Monitoring of Pollution (TEMPO)

81   satellite instrument will provide hourly observations of air quality relevant trace gases over

82   North America at an unprecedented spatial and temporal resolution (Zoogman et al., 2017). As is

83   the case for all nadir satellite retrievals, the quality of these observations will depend on the

84   accuracy of the surface reflectance used in the retrieval. As a significant portion of the observed

85   domain experiences snow cover, an accurate representation of snow cover is needed. Current

86   plans to deal with snow cover for TEMPO are to rely on external observations.

In this work, we examine the importance of accurate snow identification by using a radiative transport model to evaluate how the vertical sensitivity of a satellite retrieval is impacted by surface reflectance. We then assess seven snow extent products that are expected to continue to be operational during the TEMPO mission using in situ observations across North America with the intent of determining which product is best suited for providing snow cover information for TEMPO and other future satellite retrievals. Finally, we combine radiative transfer model results with a snow extent product to show how including snow-covered scenes improves both the quantity and quality of information in a retrieval data set.

2. Data and algorithms

2.1. Gridded snow products

2.1.1. IMS

One of the most widely used sources of snow extent data is the Interactive Multisensor Snow and Ice Mapping System (IMS). IMS provides daily, near-real-time maps of snow and sea ice cover in the Northern Hemisphere at 4 km resolution (Helfrich et al., 2007). The maps are produced by a trained analyst using visible imagery from a collection of geostationary (e.g. GOES, MeteoSat) and polar orbiting (e.g. AVHRR, MODIS, SAR) satellite instruments, with additional information from microwave sensors (e.g. DMSP, AMSR, AMSU), surface observations (e.g. SNOTEL), and models (e.g. SNODAS) (Helfrich et al., 2007). By using multiple sources of information with different spatial resolution and temporal sampling, IMS can minimize interference from clouds.

2.1.2. MODIS

A second commonly used snow and ice product is derived from MODIS satellite observations from the Terra and Aqua satellites (Hall and Riggs, 2007). Terra and Aqua have sun-synchronous, near-polar orbits with overpass times of 1030 and 1330, respectively. Snow cover is calculated using a Normalized Difference Snow Index (NDSI), which examines the difference between observed radiation at visible wavelengths (where snow is highly reflective) and short infrared wavelengths (where there is little reflection from snow). Observations are

115 made at 500 m spatial resolution and aggregated to produce daily snow cover fractions on a

116 0.05° resolution grid. Past evaluations of the standard MODIS snow product show good

117 agreement in cloud-free conditions but often snow is misidentified as cloud (Hall and Riggs,

118 2007; Yang et al., 2015).

119   The Multiangle Implementation of Atmospheric Correction (MAIAC) algorithm is

120 another algorithm processing MODIS observations. MAIAC retrievals uses radiances observed

121 by the MODIS Aqua and Terra satellites to provide atmospheric and surface products including

122 snow detection on a 1 km grid (Lyapustin et al., 2011a, 2011b, 2012). While the NDSI used by

123 the standard MODIS product is also used by MAIAC as one of the criteria, the overall snow and

124 cloud detection in MAIAC are different from the standard MODIS algorithm (Lyapustin et al.,

125 2008).

126   **2.1.3. NISE**

127   The Near-real-time Ice and Snow Extent (NISE) provides daily updated snow cover

128 extent information on a 25x25 km grid (Nolin et al., 2005). NISE uses microwave measurements

129 from the Special Sensor Microwave Imager/Sounder (SSM/I) on a sun-synchronous, quasi-polar

130 orbit to observe how microwave radiation emitted by soil is scattered by snow. Products based

131 on microwave measurements such as NISE are known to miss wet and thin snow, as wet snow

132 emits microwave radiation similar to soil, and thin snow does not provide sufficient scattering.

133   **2.1.4. CMC**

134   The Canadian Meteorological Centre (CMC) Daily Snow Depth Analysis Data is a

135 statistical interpolation of snow depth measurements from 8,000 surface sites across Canada and

136 U.S. interpolated using a snow pack model (Brasnett, 1999). Unlike the aforementioned satellite

137 products that provide snow extent, CMC provides snow depths. Daily snow maps are produced

138 at 25 km resolution. As it a reanalysis product, there is a time delay in availability. The CMC

139 snow depths show good agreement with independent observations over midlatitudes and is

140 considered an improvement over previous snow depth climatologies (Brown et al., 2003).

141   **2.2 Surface observations**

142   These snow identification products are evaluated against surface station observations
143   from the Global Historical Climatology Network Daily (GHCN-D) database, an amalgamation of
144   daily climate records from over 80,000 surface stations worldwide (Menne et al., 2012a). Most
145   observations over Canada and the United States are collected by government organizations
146   (Environment and Climate Change Canada and NOAA National Climatic Data Center,
147   respectively) with additional measurements from smaller observation networks. While the focus
148   of the database is collecting temperature and precipitation measurements, many stations (1,279 in
149   Canada and 13,932 in the United States in 2015 used here) also offer snow depth measurements.

150   A subset of the surface stations included in GHCN-D may also be used in the CMC
151   reanalysis. It is difficult to definitively know which stations are used, as CMC does not routinely
152   archive this information. However, we estimate that only 5% of the GHCN-D stations used here
153   are located within 0.1° of a possible CMC station, and thus GHCN-D has sufficient independent
154   information sources to evaluate the CMC product.

155   **2.3 Radiative transfer calculations**

156   The sensitivity of satellite observations of NO_2 to its vertical distribution is calculated
157   here using the LIDORT radiative transfer model (Spurr, 2002). The model is used to calculate
158   scattering weights, which quantify the sensitivity of backscattered solar radiation to NO_2 at
159   different altitudes (Martin et al., 2002; Palmer et al., 2001). The observation sensitivity to lower
160   tropospheric NO_2 is represented by the AMF. AMFs for OMI satellite observations in January
161   2013 are calculated as a useful analog for future TEMPO observations as both instruments are
162   spectrometers observing reflected sunlight at UV to visible wavelengths. AMFs are calculated at
163   440 nm, at the centre of the NO_2 retrieval window for OMI and TEMPO where NO_2 has strong
164   absorption features. Vertical NO_2 profiles, as well as other trace gas and aerosol profiles needed
165   for the AMF calculation shown here, are obtained from a simulation of the GEOS-Chem
166   chemical transport model version 11-01 (www.geos-chem.org).

167   Figure 1 shows maps of snow-free and snow-covered reflectances used here. Snow-free
168   surface reflectance at 470 nm is provided by Nadir BRDF-Adjusted reflectances from the
169   MODIS CMG Gap-Filled Snow-Free Products (Sun et al., 2017). Reflectivities at 354 nm for
170   snow-covered scenes are derived from OMI observations as described by O'Byrne et al. (2010).
171   This data set is consistent with previous snow reflectivity (e.g. Moody et al., 2007; Tanskanen

172   and Manninen, 2007) over most land types (O'Byrne et al., 2010). Snow-covered reflectivity has

173   an estimated uncertainty of 10-20% in most regions, with higher uncertainties in regions with

174   thin or transient snow. Although the 354 nm wavelength is different than the 440 nm wavelength

175   used to calculate AMFs, snow reflectivity has weak spectral dependence in UV-visible

176   wavelengths (Feister and Grewe, 1995; O'Byrne et al., 2010). Snow can increase surface

177   reflectance by over a factor of 10 in central North America where short vegetation is readily

178   covered by snow.

179   **3. Methods**

180   Here we test daily snow cover products for 2015. Snow products are regridded from their

181   native resolutions to a common 4 km grid (similar to the spatial resolution of TEMPO). A grid

182   box is considered to be snow covered if any observations within that box are snow covered.

183   MAIAC, NISE, and IMS give only a yes or no flag for presence of snow. MODIS products

184   provide a pixel snow fraction, and we consider any pixels with nonzero snow fractions as snow

185   covered. Any CMC grid box with nonzero snow depth is considered snow covered.

186   GHCN-D surface measurements are used as the ground "truth" for evaluating the satellite

187   and reanalysis snow data products tested here. If measurements from multiple surface data

188   networks exist in the same grid box, the most reliable source is used per the priority order given

189   by GHCN-D (Menne et al., 2012b). If observations from multiple surface stations within the

190   most reliable network within a grid box disagree on the presence of snow on a given day, that

191   day is excluded from the evaluation.

192   We assess the snow data sets using metrics that are commonly used for evaluating binary

193   data sets (Rittger et al., 2013). These metrics are based on the possible outcomes for identifying

194   snow: true positive (TP), true negative (TN), false positive (FP), and false negative (FN).

195   Accuracy measures the likelihood that a grid box, with snow or without, is correctly classified:

$$Accuracy = \frac{TP + TN}{TP + TN + FP + FN} \tag{1}$$

196   Precision is the probability that a region identified as snow covered has snow:

$$Precision = \frac{TP}{TP + FP} \tag{2}$$

197   Recall is the likelihood that snow cover is detected when present:

$$Recall = \frac{TP}{TP + FN} \tag{3}$$

198 The *F* score balances recall (which accounts for false negatives) and precision (which accounts

199 for false positives) to measure correct classification of snow without the influence of frequent

200 snow-free periods, and it is therefore the metric which is most relevant for TEMPO:

$$F = 2 * \frac{precision * recall}{precision + recall} \tag{4}$$

4. Results

201

202 We first examine the effect of surface reflectivity on retrieval sensitivity by using the

203 LIDORT radiative transfer model to calculate NO_2 AMFs for both snow-free and snow-covered

204 scenarios using the corresponding snow-free (Sun et al., 2017) or snow-covered (O'Byrne et al.,

205 2010) surface reflectance over North America. We calculate AMFs over North America in

206 January 2013. We assume cloud-free conditions in all AMF calculations, as the impact of surface

207 reflectance on retrieved cloud fractions is beyond the scope of this paper.

208 Figure 2 shows the sensitivity of backscattered radiation (scattering weights) over snow-

209 covered and snow-free surfaces for two locations: a midlatitude location (US Midwest: 42°N,

210 99°W) with a solar zenith angle of 60° and at a high-latitude location (Northern Canada: 58°N,

211 76°W) with a solar zenith angle of 79°. The snow-covered scattering weights are greater than the

212 snow-free scattering weights throughout the troposphere, by factors of 2.0 (2.7) below 5 km, 2.7

213 (3.7) below 2 km, and 2.6 (5.3) below 1 km at the mid- (high-) latitude location. This shows that

214 satellite-observed backscattered radiation in clear-sky conditions is up to 5 times as sensitive to

215 NO_2 in the boundary layer after accounting for increased reflection by snow, due to the increased

216 absorption by NO_2 in the lower troposphere when the surface reflects more sunlight.

217 Figure 3 shows the distribution of AMF values over North America with and without

218 reflectance from snow. The snow-free AMF distribution is unimodal with a median of 1.2.

219 Allowing for the presence of snow introduces a second mode with a median of 3.2. Mean AMFs

220 increase by a factor of 2.0 in the presence of snow, indicating an overall doubling in the

221 sensitivity to tropospheric NO_2 over snow-covered surfaces across North America. The impact is

222 larger over polluted regions, as mean AMFs increase by a factor of 2.2 in regions where NO_2

223   columns exceed 1×10^{15} molec/cm^2. Maps of AMF with and without snow cover for January 2013

224   show that AMF values increase over 69% of the land surface within the TEMPO domain.

225   We next examine the snow datasets to identify the one most suited for the TEMPO

226   retrieval algorithm. Figure 4 shows the spatial distribution of false positives and false negatives

227   in the data sets. In all data sets, both false positives and negatives are most frequent over

228   mountainous regions, particularly in the Rocky Mountain region, consistent with previous

229   validation studies (Chen et al., 2012, 2014; Frei et al., 2012; Frei and Lee, 2010). These errors

230   are often attributed to differences in representativeness, as snow cover in mountain regions is

231   often spatially inhomogeneous, and thus *in situ* measurements may not be representative of the

232   pixel. A slight increase in the number of false positives in IMS over mid-western and prairie

233   regions may result from crop regions with high snow-free albedos being mistaken for snow in

234   visible imagery (Chen et al., 2012; Yang et al., 2015). NISE, MODIS Aqua, and MODIS Terra

235   have more false negatives overall, especially in the Great Lakes and New England regions. False

236   positives are less frequent than false negatives in all data sets. IMS and CMC have the lowest

237   frequency of false negatives. NISE and MAIAC have the lowest frequency of false positives.

238   Figure 5 shows the metrics used to evaluate data set performance. Table 1 summarizes

239   these results. All data sets have high accuracy numbers, owing largely to a high number of true

240   negatives during the summer months. MODIS Aqua and Terra have low recall and *F* scores.

241   When only observations with MODIS cloud fractions less than 20% are used, MODIS has better

242   agreement with the ground stations (*F* statistic increases from 0.38 to 0.49 at native resolution

243   for Aqua, 0.43 to 0.63 for Terra), but this reduces the number of usable MODIS observations by

244   up to 60%. NISE has high precision but low recall, indicating that while areas classified as snow-

245   covered by NISE are likely correct, many snow-covered regions are missing in the data set. This

246   is consistent with evaluations by McLinden et al. (2014) and O'Byrne et al. (2010). Although

247   CMC, IMS, and MAIAC products show an increase in frequency of false negatives over the

248   Rocky Mountains, they retain a high precision in this region due to frequent snow cover. While

249   MAIAC Aqua and Terra have high accuracy and precision, lower recall values indicate that they

250   are conservative in identifying the presence of snow. This is possibly a consequence of the

251   method used for identifying cloud, which may incorrectly classify fresh snowfall as cloud

252   (Lyapustin et al., 2008). Data sets were also evaluated by season with similar results (Appendix

253   Table A1). All data sets have weaker performance metrics during the spring melt season, which

254   has been observed in past evaluations (Frei et al., 2012). IMS has the highest *F* score in winter

255   and autumn but is slightly outperformed by MAIAC in spring. Data sets were also evaluated at

256   their native resolutions and at a common 25 km resolution (Appendix Tables A2-3). Results are

257   similar at each resolution with two exceptions: MODIS Aqua and Terra products perform better

258   when regridded from their native 0.05° resolution to a 4 km resolution as it reduces the number

259   of grid boxes missing observations due to cloud, and MAIAC Aqua and Terra perform better at

260   their native resolution than at either 4 km or 25 km as degrading the spatial resolution results in a

261   loss of information.

262   For all data sets, recall is generally low in two regions: along the Pacific coastline where

263   snow depths are relatively thin and in the south when snow is rare and generally short lived. Thin

264   snow is likely to be less homogenous across a pixel and more likely to be obscured by forest

265   canopies or tall grasses, and thus is difficult to observe from satellite imagery. Short-lived snow

266   in the south is likely to be missed by satellite observations, especially since clouds are often

267   present. However, as IMS uses multiple observations at multiple times of day in addition to

268   incorporating ground station data, it is more likely to find snow in these cases than other satellite

269   products (Hall et al., 2010). Overall, IMS has best agreement with *in situ* observations, with the

270   highest accuracy, recall, and *F* statistic and relatively high precision.

271   While CMC also has strong performance metrics, it is important to consider the

272   information source used to describe snow extent in each product. Products based on satellite

273   observations are advantageous when assessing how surface reflectivity affects backscattered

274   radiation observed from space. For example, thin snow, or snow obscured by tree canopies, may

275   not affect the observed brightness from space, but would be considered snow-covered by a

276   product based on surface observations (e.g. CMC). Also, the reflectivity of a snow-covered

277   surface decreases over time as the snow ages (Warren and Wiscombe, 1980); This effect would

278   not be captured by snow depth measurements. Additionally, while snow depth has been used as

279   an indicator of brightness (Arola et al., 2003), it cannot account for snow aging or canopy

280   effects. IMS is based on visible satellite imagery and thus determines snow extent based on

281   brightness from space, which is more applicable to satellite retrievals. And while most satellite-

282   based products rely on observations made at a single overpass time and viewing geometry, IMS

283   has the advantage of incorporating observations from multiple satellites with differing

284   measurement times and geometries, including both geostationary and low Earth orbits. These

285   reasons, in addition to a strong agreement with in situ measurements and near-real-time updates,

286   make IMS best suited for informing TEMPO retrievals.

287   We next examine the effect on both spatial sampling and sensitivity to the lower

288   troposphere of a retrieval data set if observations with surface snow are included rather than

289   omitted. We use IMS to identify the presence of snow for OMI observations over North America

290   in January 2015. We then use LIDORT to calculate AMFs for these observations using the

291   corresponding snow-free (Sun et al., 2017) or snow-covered (O'Byrne et al., 2010) surface

292   reflectance and examine the results of either including or omitting snow-covered scenes. Figure 6

293   shows that including snow-covered scenes results in a significant (factor of 2.1) increase in

294   observation frequency, particularly in the northern US and Canada. Additionally, including

295   snow-covered scenes increases the average AMF by a factor of 2.7 in regions with occasional

296   snow cover. The increase in AMF demonstrates that including snow-covered scenes increases

297   the quality of information about the tropospheric NO_2 column by increasing the observation

298   sensitivity to tropospheric NO_2. As we assume clear-sky conditions, these are likely upper

299   bounds on potential increases in observation quantity and quality. In practice, the presence of

300   clouds and errors in cloud retrieval algorithms will likely diminish these impacts.

301

302   5. Conclusion

303   An accurate representation of snow cover is essential to ensuring satellite retrieval

304   accuracy, including those from TEMPO. Radiative transfer model calculations indicate that

305   clear-sky NO_2 retrievals over reflective snow-covered surfaces are more than twice as sensitive

306   to NO_2 in the boundary layer than over snow-free surfaces. This makes snow an attractive

307   surface over which to observe tropospheric NO_2. However, the lack of confidence in snow

308   identification has previously led many retrieval procedures to omit observations over snow. We

309   show that increasing this confidence such that these observations could be included not only

310   improves spatial and temporal sampling but also allows the inclusion of observations with

311   higher-quality information on the lower troposphere.

312   We evaluated seven snow extent data sets to determine their usefulness for informing

313   satellite retrievals of trace gas from solar backscatter observations. All products were more likely

314   to misidentify snow over mountains or where snow cover is thin or short lived. IMS had the best

315   agreement with *in situ* observations (F=0.85), and as a satellite-based, operational, daily updated

316   product, it is well suited for informing TEMPO satellite retrievals. The low recall value (0.45)

317   for NISE indicated that a significant number of snow-covered pixels are missed. The standard

318   MODIS products showed medium precision and low recall owing to cloud contamination. The

319   MAIAC products had the highest precision (0.90 for both Aqua and Terra) of those tested, but is

320   conservative in ascribing the presence of snow (recall of 0.74 for Aqua, 0.75 for Terra). CMC

321   had strong performance metrics (F=0.81), but as a reanalysis product based on ground

322   observations it may not appropriately represent how a surface snow reflectivity would affect

323   TEMPO-observed radiances.

324   The potential improvements in NO_2 retrieval performance over snow-covered scenes

325   outlined here were tested for clear-sky conditions. The accuracy of cloud retrieval schemes also

326   impacts the quality of trace gas retrievals. Many cloud retrieval schemes have difficulty

327   distinguishing between a bright surface and bright, low-altitude clouds; This may diminish the

328   impact that improved surface snow reflectance can have on observation frequency and sensitivity

329   when clouds are present. However, using accurate surface snow cover information may also lead

330   to corresponding improvements in cloud retrieval accuracy.

331   Future work should investigate snow reflectance products that could be used when snow

332   is detected. This could potentially include BRDFs that describe reflection at different viewing

333   angles, as this effect has been shown to have significant impact on retrieved NO_2 columns and

334   clouds (Lorente et al., 2018; Vasilkov et al., 2017). Accurate knowledge of snow reflectivity is

335   also needed to improve retrievals over snow. A retrieval algorithm that combines daily snow

336   detection from IMS with a climatology of snow reflectance has the potential to greatly improve

337   upon current methodologies.

338

339   **6. Data Availability**

340   IMS (https://doi.org/10.7265/N52R3PMC, National Ice Center, 2008), NISE

341   (https://doi.org/10.5067/3KB2JPLFPK3R, Brodzik and Stewart, 2016), MODIS Aqua

342   (https://doi.org/10.5067/MODIS/MYD10C1.006, Hall and Riggs, 2016a), MODIS Terra

343   (https://doi.org/10.5067/MODIS/MOD10C1.006, Hall and Riggs, 2016b), and CMC (Brown and

344   Brasnett, 2010) data are available from the NASA National Snow and Ice Data Center

345   (http://nsidc.org, last access: 17 July 2017). MAIAC Collection 6 (Lyapustin et al., 2011a, b,

346   2012) re-processing of MODIS data started in September 2017 and is expected to be completed

347   by the end of year. This study used MAIAC Atmospheric Properties files currently available via

348   ftp at the NASA Center for Climate Simulations (NCCS):

349   ftp://maiac@dataportal.nccs.nasa.gov/DataRelease/ (last access: 15 June 2017). GHCN-D data

350   are available from the NOAA National Climatic Data Center

351   https://doi.org/10.7289/V5D21VHZ, Menne et al., 2012b). AMF code (Spurr, 2002; Martin et

352   al., 2002) used to calculate scattering weights and air mass factors, as well as snow-covered

353   Surface LER (O'Byrne et al., 2010) used here, is available at http://fizz.phys.dal.ca/~atmos (last

354   access: 19 June 2017) MODIS MCD43GF CMG Gap-Filled Snow-free surface reflectances (Sun

355   et al., 2017) are available at ftp://rsftp.eeos.umb.edu/data02/Gapfilled/ (Sun et al., 2017). The

356   GEOS-Chem chemical transport model used here is available at www.geos-chem.org (last

357   access: 15 June 2017).

7. References

359   Arola, A., Kaurola, J., Koskinen, L., Tanskanen, A., Tikkanen, T., Taalas, P., Herman, J. R.,

360   Krotkov, N. and Fioletov, V.: A new approach to estimating the albedo for snow-covered

361   surfaces in the satellite UV method, J. Geophys. Res., 108(D17), 4531,

362   doi:10.1029/2003JD003492, 2003.

363   Beirle, S., Boersma, K. F., Platt, U., Lawrence, M. G. and Wagner, T.: Megacity emissions and

364   lifetimes of nitrogen oxides probed from space., Science, 333(6050), 1737–9,

365   doi:10.1126/science.1207824, 2011.

366   Boersma, K. F., Eskes, H. J. and Brinksma, E. J.: Error analysis for tropospheric NO2 retrieval

367   from space, J. Geophys. Res. Atmos., 109(D4), 2004.

368   Brasnett, B.: A Global Analysis of Snow Depth for Numerical Weather Prediction, J. Appl.

369   Meteorol., 38(6), 726–740, doi:10.1175/1520-0450(1999)038<0726:AGAOSD>2.0.CO;2, 1999.

370   Brodzik, M. J. and Stewart, J. S.: Near-Real-Time SSM/I-SSMIS EASE-Grid Daily Global Ice

371   Concentration and Snow Extent, Version 5, , doi:http://dx.doi.org/10.5067/3KB2JPLFPK3R,

372   2016.

373   Brown, R. D. and Brasnett, B.: Canadian Meteorological Centre (CMC) Daily Snow Depth

374   Analysis Data, Version 1, , doi:http://dx.doi.org/10.5067/W9FOYWH0EQZ3, 2010.

375   Brown, R. D., Brasnett, B. and Robinson, D.: Gridded North American monthly snow depth and

376   snow water equivalent for GCM evaluation, Atmosphere-Ocean, 41(1), 1–14,

377   doi:10.3137/ao.410101, 2003.

378   Chen, C., Lakhankar, T., Romanov, P., Helfrich, S., Powell, A. and Khanbilvardi, R.: Validation

379   of NOAA-Interactive Multisensor Snow and Ice Mapping System (IMS) by Comparison with

380   Ground-Based Measurements over Continental United States, Remote Sens., 4(12), 1134–1145,

381   doi:10.3390/rs4051134, 2012.

382   Chen, X., Jiang, L., Yang, J. and Pan, J.: Validation of ice mapping system snow cover over

383   southern China based on Landsat Enhanced Thematic Mapper Plus imagery, J. Appl. Remote

384   Sens., 8(1), 84680, doi:10.1117/1.JRS.8.084680, 2014.

385   Duncan, B. N., Prados, A. I., Lamsal, L. N., Liu, Y., Streets, D. G., Gupta, P., Hilsenrath, E.,

386   Kahn, R. A., Nielsen, J. E., Beyersdorf, A. J., Burton, S. P., Fiore, A. M., Fishman, J., Henze, D.

387   K., Hostetler, C. A., Krotkov, N. A., Lee, P., Lin, M., Pawson, S., Pfister, G., Pickering, K. E.,

388   Pierce, R. B., Yoshida, Y. and Ziemba, L. D.: Satellite data of atmospheric pollution for U.S. air

389   quality applications: Examples of applications, summary of data end-user resources, answers to

390   FAQs, and common mistakes to avoid, Atmos. Environ., 94, 647–662,

391   doi:10.1016/j.atmosenv.2014.05.061, 2014.

392   Feister, U. and Grewe, R.: Spectral albedo measurements in the UV and visible region over

393   different types of surfaces, Photochem. Photobiol., 62(4), 736–744, doi:10.1111/j.1751-

394   1097.1995.tb08723.x, 1995.

395   Fioletov, V. E., McLinden, C. A., Krotkov, N. and Li, C.: Lifetimes and emissions of SO2 from

396   point sources estimated from OMI, Geophys. Res. Lett., 42(6), 1969–1976,

doi:10.1002/2015GL063148, 2015.

Fishman, J., Al-Saadi, J. A., Creilson, J. K., Bowman, K. W., Burrows, J. P., Richter, A., Chance, K. V., Edwards, D. P., Martin, R. V., Morris, G. A., Pierce, R. B., Ziemke, J. R., Schaack, T. K., Thompson, A. M., Fishman, J., Al-Saadi, J. A., Creilson, J. K., Bowman, K. W., Burrows, J. P., Richter, A., Chance, K. V., Edwards, D. P., Martin, R. V., Morris, G. A., Pierce, R. B., Ziemke, J. R., Schaack, T. K. and Thompson, A. M.: Remote Sensing of Tropospheric Pollution from Space, Bull. Am. Meteorol. Soc., 89(6), 805–821, doi:10.1175/2008BAMS2526.1, 2008.

de Foy, B., Lu, Z., Streets, D. G., Lamsal, L. N. and Duncan, B. N.: Estimates of power plant NO x emissions and lifetimes from OMI NO 2 satellite retrievals, Atmos. Environ., 116, 1–11, 2015.

Frei, A. and Lee, S.: A comparison of optical-band based snow extent products during spring over North America, Remote Sens. Environ., 114(9), 1940–1948, doi:10.1016/j.rse.2010.03.015, 2010.

Frei, A., Tedesco, M., Lee, S., Foster, J., Hall, D. K., Kelly, R. and Robinson, D. A.: A review of global satellite-derived snow products, Adv. Sp. Res., 50(8), 1007–1029, doi:10.1016/j.asr.2011.12.021, 2012.

Geddes, J. A. and Martin, R. V.: Global deposition of total reactive nitrogen oxides from 1996 to 2014 constrained with satellite observations of NO2 columns, Atmos. Chem. Phys., 17(16), 10071–10091, doi:10.5194/acp-17-10071-2017, 2017.

Hall, D. . and Riggs, G. A.: MODIS/Aqua Snow Cover Daily L3 Global 0.05Deg CMG, Version 6, , doi:http://dx.doi.org/10.5067/MODIS/MYD10C1.006, 2016a.

Hall, D. K. and Riggs, G. A.: Accuracy assessment of the MODIS snow products, Hydrol. Process., 21(12), 1534–1547, doi:10.1002/hyp.6715, 2007.

Hall, D. K. and Riggs, G. A.: MODIS/Terra Snow Cover Daily L3 Global 0.05Deg CMG, Version 6, , doi:http://dx.doi.org/10.5067/MODIS/MOD10C1.006, 2016b.

Hall, D. K., Fuhrmann, C. M., Perry, L. B., Riggs, G. A., Robinson, D. A. and Foster, J. L.: A Comparison of Satellite-Derived Snow Maps with a Focus on Ephemeral Snow in North Carolina, in 67th Eastern Snow Conference, Hancock MA USA., 2010.

425 Helfrich, S. R., McNamara, D., Ramsay, B. H., Baldwin, T. and Kasheta, T.: Enhancements to,

426 and forthcoming developments in the Interactive Multisensor Snow and Ice Mapping System

427 (IMS), Hydrol. Process., 21(12), 1576–1586, doi:10.1002/hyp.6720, 2007.

428 Herman, J. R. and Celarier, E. A.: Earth surface reflectivity climatology at 340-380 nm from

429 TOMS data, J. Geophys. Res. Atmos., 102(D23), 28003–28011, doi:10.1029/97JD02074, 1997.

430 Kleipool, Q. L., Dobber, M. R., de Haan, J. F. and Levelt, P. F.: Earth surface reflectance

431 climatology from 3 years of OMI data, J. Geophys. Res., 113(D18), D18308,

432 doi:10.1029/2008JD010290, 2008.

433 Koelemeijer, R. B. A., de Haan, J. F. and Stammes, P.: A database of spectral surface reflectivity

434 in the range 335–772 nm derived from 5.5 years of GOME observations, J. Geophys. Res.,

435 108(D2), 4070, doi:10.1029/2002JD002429, 2003.

436 Lamsal, L. N., Janz, S. J., Krotkov, N. A., Pickering, K. E., Spurr, R. J. D., Kowalewski, M. G.,

437 Loughner, C. P., Crawford, J. H., Swartz, W. H. and Herman, J. R.: High-resolution NO2

438 observations from the Airborne Compact Atmospheric Mapper: Retrieval and validation, J.

439 Geophys. Res. Atmos., 122(3), 1953–1970, doi:10.1002/2016JD025483, 2017.

440 Liang, S., Fang, H., Chen, M., Shuey, C. J., Walthall, C., Daughtry, C., Morisette, J., Schaaf, C.

441 and Strahler, A.: Validating MODIS land surface reflectance and albedo products: methods and

442 preliminary results, Remote Sens. Environ., 83(1–2), 149–162, doi:10.1016/S0034-

443 4257(02)00092-5, 2002.

444 Lin, J.-T., Liu, M.-Y., Xin, J.-Y., Boersma, K. F., Spurr, R., Martin, R. and Zhang, Q.: Influence

445 of aerosols and surface reflectance on satellite NO2 retrieval: seasonal and spatial characteristics

446 and implications for NOx emission constraints, Atmos. Chem. Phys., 15(19), 11217–11241,

447 doi:10.5194/acp-15-11217-2015, 2015.

448 Lorente, A., Folkert Boersma, K., Yu, H., Dörner, S., Hilboll, A., Richter, A., Liu, M., Lamsal,

449 L. N., Barkley, M., De Smedt, I., Van Roozendael, M., Wang, Y., Wagner, T., Beirle, S., Lin, J.-

450 T., Krotkov, N., Stammes, P., Wang, P., Eskes, H. J. and Krol, M.: Structural uncertainty in air

451 mass factor calculation for NO2 and HCHO satellite retrievals, Atmos. Meas. Tech., 10(3), 759–

452 782, doi:10.5194/amt-10-759-2017, 2017.

453 Lorente, A., Boersma, K. F., Stammes, P., Tilstra, L. G., Richter, A., Yu, H., Kharbouche, S. and

454 Muller, J.-P.: The importance of surface reflectance anisotropy for cloud and NO2 retrievals

455 from GOME-2 and OMI, Atmos. Meas. Tech. Discuss., 1–29, doi:10.5194/amt-2018-32, 2018.

456 Lyapustin, A., Wang, Y. and Frey, R.: An automatic cloud mask algorithm based on time series

457 of MODIS measurements, J. Geophys. Res., 113(D16), D16207, doi:10.1029/2007JD009641,

458 2008.

459 Lyapustin, A., Martonchik, J., Wang, Y., Laszlo, I. and Korkin, S.: Multiangle implementation of

460 atmospheric correction (MAIAC): 1. Radiative transfer basis and look-up tables, J. Geophys.

461 Res., 116(D3), D03210, doi:10.1029/2010JD014985, 2011a.

462 Lyapustin, A., Wang, Y., Laszlo, I., Kahn, R., Korkin, S., Remer, L., Levy, R. and Reid, J. S.:

463 Multiangle implementation of atmospheric correction (MAIAC): 2. Aerosol algorithm, J.

464 Geophys. Res., 116(D3), D03211, doi:10.1029/2010JD014986, 2011b.

465 Lyapustin, A. I., Wang, Y., Laszlo, I., Hilker, T., G.Hall, F., Sellers, P. J., Tucker, C. J. and

466 Korkin, S. V.: Multi-angle implementation of atmospheric correction for MODIS (MAIAC): 3.

467 Atmospheric correction, Remote Sens. Environ., 127, 385–393, doi:10.1016/j.rse.2012.09.002,

468 2012.

469 Martin, R. V, Chance, K., Jacob, D. J., Kurosu, T. P., Spurr, R. J. D., Bucsela, E., Gleason, J. F.,

470 Palmer, P. I., Bey, I. and Fiore, A. M.: An improved retrieval of tropospheric nitrogen dioxide

471 from GOME, J. Geophys. Res. Atmos., 107(D20), 2002.

472 Martin, R. V.: Satellite remote sensing of surface air quality, Atmos. Environ., 42(34), 7823–

473 7843, doi:10.1016/j.atmosenv.2008.07.018, 2008.

474 McLinden, C. A., Fioletov, V., Boersma, K. F., Kharol, S. K., Krotkov, N., Lamsal, L., Makar,

475 P. A., Martin, R. V., Veefkind, J. P. and Yang, K.: Improved satellite retrievals of NO2 and SO2

476 over the Canadian oil sands and comparisons with surface measurements, Atmos. Chem. Phys.,

477 14(7), 3637–3656, doi:10.5194/acp-14-3637-2014, 2014.

478 Menne, M. J., Durre, I., Vose, R. S., Gleason, B. E., Houston, T. G., Menne, M. J., Durre, I.,

479 Vose, R. S., Gleason, B. E. and Houston, T. G.: An Overview of the Global Historical

480 Climatology Network-Daily Database, J. Atmos. Ocean. Technol., 29(7), 897–910,

481   doi:10.1175/JTECH-D-11-00103.1, 2012a.

482   Menne, M. J., Durre, I., Korzeniewski, B., McNeal, S., Thomas, K., Yin, X., Anthony, S., Ray,

483   R., Vose, R. S., Gleason, B. E. and Houston, T. G.: Global Historical Climatology Network -

484   Daily (GHCN-Daily), Version 3.22, , doi:http://doi.org/10.7289/V5D21VHZ, 2012b.

485   Moody, E. G., King, M. D., Schaaf, C. B., Hall, D. K. and Platnick, S.: Northern Hemisphere

486   five-year average (2000–2004) spectral albedos of surfaces in the presence of snow: Statistics

487   computed from Terra MODIS land products, Remote Sens. Environ., 111(2), 337–345,

488   doi:10.1016/j.rse.2007.03.026, 2007.

489   National Ice Center: IMS Daily Northern Hemisphere Snow and Ice Analysis at 1 km, 4 km, and

490   24 km Resolutions, Version 1, , doi:http://dx.doi.org/10.7265/N52R3PMC, 2008.

491   Nolin, A., Armstrong, R. and Maslanik, J.: Near real-time SSM/I EASE-grid daily global ice

492   concentration and snow extent, Digit. Media, Natl. Snow Ice Data Center, Boulder, CO, USA,

493   2005.

494   Nowlan, C. R., Martin, R. V., Philip, S., Lamsal, L. N., Krotkov, N. A., Marais, E. A., Wang, S.

495   and Zhang, Q.: Global dry deposition of nitrogen dioxide and sulfur dioxide inferred from space-

496   based measurements, Global Biogeochem. Cycles, 28(10), 1025–1043,

497   doi:10.1002/2014GB004805, 2014.

498   O'Byrne, G., Martin, R. V., van Donkelaar, A., Joiner, J. and Celarier, E. A.: Surface reflectivity

499   from the Ozone Monitoring Instrument using the Moderate Resolution Imaging

500   Spectroradiometer to eliminate clouds: Effects of snow on ultraviolet and visible trace gas

501   retrievals, J. Geophys. Res., 115(D17), D17305, doi:10.1029/2009JD013079, 2010.

502   Palmer, P. I., Jacob, D. J., Chance, K. and Martin, R. V: Air mass factor formulation for

503   spectroscopic measurements from satellites' Application to formaldehyde retrievals from the

504   Global Ozone Monitoring Experiment, J. Geophys. Res., 106(D13), 14,514-539,550 [online]

505   Available from: https://agupubs.onlinelibrary.wiley.com/doi/full/10.1029/2000JD900772, 2001.

506   Richter, A. and Wagner, T.: The Use of UV, Visible and Near IR Solar Back Scattered Radiation

507   to Determine Trace Gases, pp. 67–121, Springer, Berlin, Heidelberg., 2011.

508   Rittger, K., Painter, T. H. and Dozier, J.: Assessment of methods for mapping snow cover from

509   MODIS, Adv. Water Resour., 51, 367–380, doi:10.1016/j.advwatres.2012.03.002, 2013.

510   Spurr, R. J. D.: Simultaneous derivation of intensities and weighting functions in a general

511   pseudo-spherical discrete ordinate radiative transfer treatment, J. Quant. Spectrosc. Radiat.

512   Transf., 75(75), 129–175 [online] Available from:

513   https://www.sciencedirect.com/science/article/pii/S002240730100245X (Accessed 20 July

514   2017), 2002.

515   Streets, D. G., Canty, T., Carmichael, G. R., de Foy, B., Dickerson, R. R., Duncan, B. N.,

516   Edwards, D. P., Haynes, J. A., Henze, D. K. and Houyoux, M. R.: Emissions estimation from

517   satellite retrievals: A review of current capability, Atmos. Environ., 77, 1011–1042, 2013.

518   Sun, Q., Wang, Z., Li, Z., Erb, A. and Schaaf, C. B.: Evaluation of the global MODIS 30 arc-

519   second spatially and temporally complete snow-free land surface albedo and reflectance

520   anisotropy dataset, Int. J. Appl. Earth Obs. Geoinf., 58, 36–49, doi:10.1016/j.jag.2017.01.011,

521   2017.

522   Tanskanen, A. and Manninen, T.: Effective UV surface albedo of seasonally snow-covered

523   lands, Atmos. Chem. Phys., 7(10), 2759–2764, doi:10.5194/acp-7-2759-2007, 2007.

524   Valin, L. C., Russell, A. R. and Cohen, R. C.: Variations of OH radical in an urban plume

525   inferred from NO2 column measurements, Geophys. Res. Lett., 40(9), 1856–1860, 2013.

526   Vasilkov, A., Qin, W., Krotkov, N., Lamsal, L., Spurr, R., Haffner, D., Joiner, J., Yang, E.-S.

527   and Marchenko, S.: Accounting for the effects of surface BRDF on satellite cloud and trace-gas

528   retrievals: a new approach based on geometry-dependent Lambertian equivalent

529   reflectivity applied to OMI algorithms, Atmos. Meas. Tech., 10(1), 333–349, doi:10.5194/amt-

530   10-333-2017, 2017.

531   Warren, S. G. and Wiscombe, W. J.: A Model for the Spectral Albedo of Snow. II: Snow

532   Containing Atmospheric Aerosols, J. Atmos. Sci., 37(12), 2734–2745, doi:10.1175/1520-

533   0469(1980)037<2734:AMFTSA>2.0.CO;2, 1980.

534   Yang, J., Jiang, L., Ménard, C. B., Luojus, K., Lemmetyinen, J. and Pulliainen, J.: Evaluation of

535   snow products over the Tibetan Plateau, Hydrol. Process., 29(15), 3247–3260,

536   doi:10.1002/hyp.10427, 2015.

537   Zoogman, P., Liu, X., Suleiman, R. M., Pennington, W. F., Flittner, D. E., Al-Saadi, J. A.,

538   Hilton, B. B., Nicks, D. K., Newchurch, M. J., Carr, J. L., Janz, S. J., Andraschko, M. R., Arola,

539   A., Baker, B. D., Canova, B. P., Chan Miller, C., Cohen, R. C., Davis, J. E., Dussault, M. E.,

540   Edwards, D. P., Fishman, J., Ghulam, A., González Abad, G., Grutter, M., Herman, J. R., Houck,

541   J., Jacob, D. J., Joiner, J., Kerridge, B. J., Kim, J., Krotkov, N. A., Lamsal, L., Li, C., Lindfors,

542   A., Martin, R. V., McElroy, C. T., McLinden, C., Natraj, V., Neil, D. O., Nowlan, C. R.,

543   O′Sullivan, E. J., Palmer, P. I., Pierce, R. B., Pippin, M. R., Saiz-Lopez, A., Spurr, R. J. D.,

544   Szykman, J. J., Torres, O., Veefkind, J. P., Veihelmann, B., Wang, H., Wang, J. and Chance, K.:

545   Tropospheric emissions: Monitoring of pollution (TEMPO), J. Quant. Spectrosc. Radiat. Transf.,

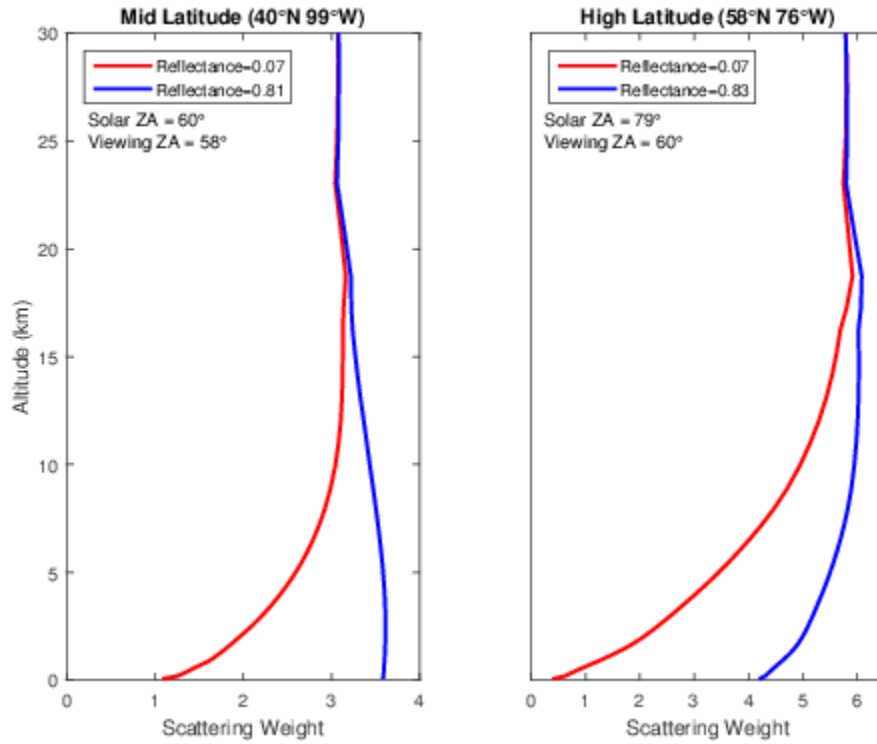546   186, 17–39, doi:10.1016/j.jqsrt.2016.05.008, 2017.

547
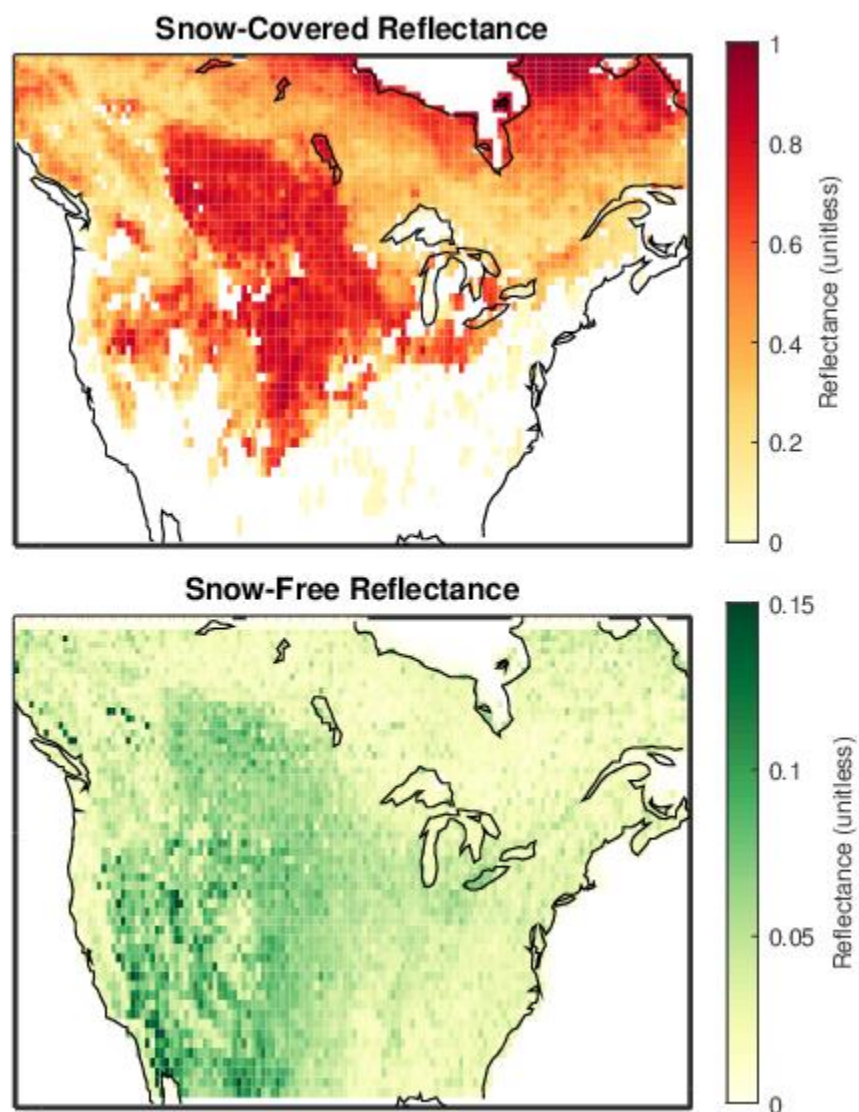
549

550 Figure 1: Surface reflectivity at UV-visible wavelengths for snow-covered and snow-free

551 conditions for January 2013. White space in top panel indicates that no snow reflectance

552 information is available.

553

554

Figure 2: Observation sensitivity to NO_2. Scattering weight profiles calculated for cloud-free

OMI NO_2 retrievals, with and without surface snow cover, for January 2013 at (Left) 42° N, 99°

W with a solar zenith angle (ZA) of 60° and (Right) 58° N, 76° W with a solar zenith angle of

79°.
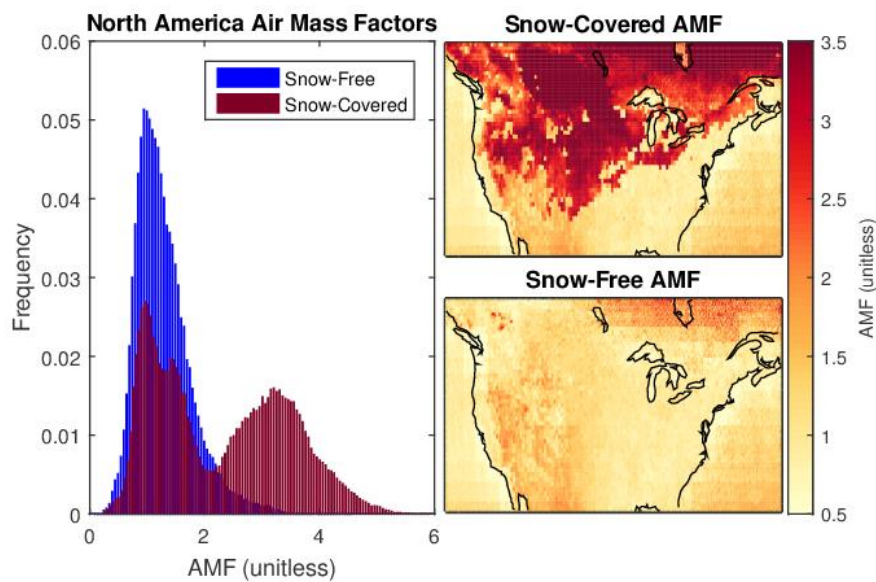
561 Figure 3: (Left) Distribution of air mass factors (AMFs) calculated for OMI NO$_2$ retrievals over

562 North America for observation geometry of January 2013, using snow-free (Sun et al., 2017) or

563 snow-covered (O'Byrne et al., 2010) surface reflectance. (Right) Maps of AMF for snow-

564 covered and snow-free conditions.

565
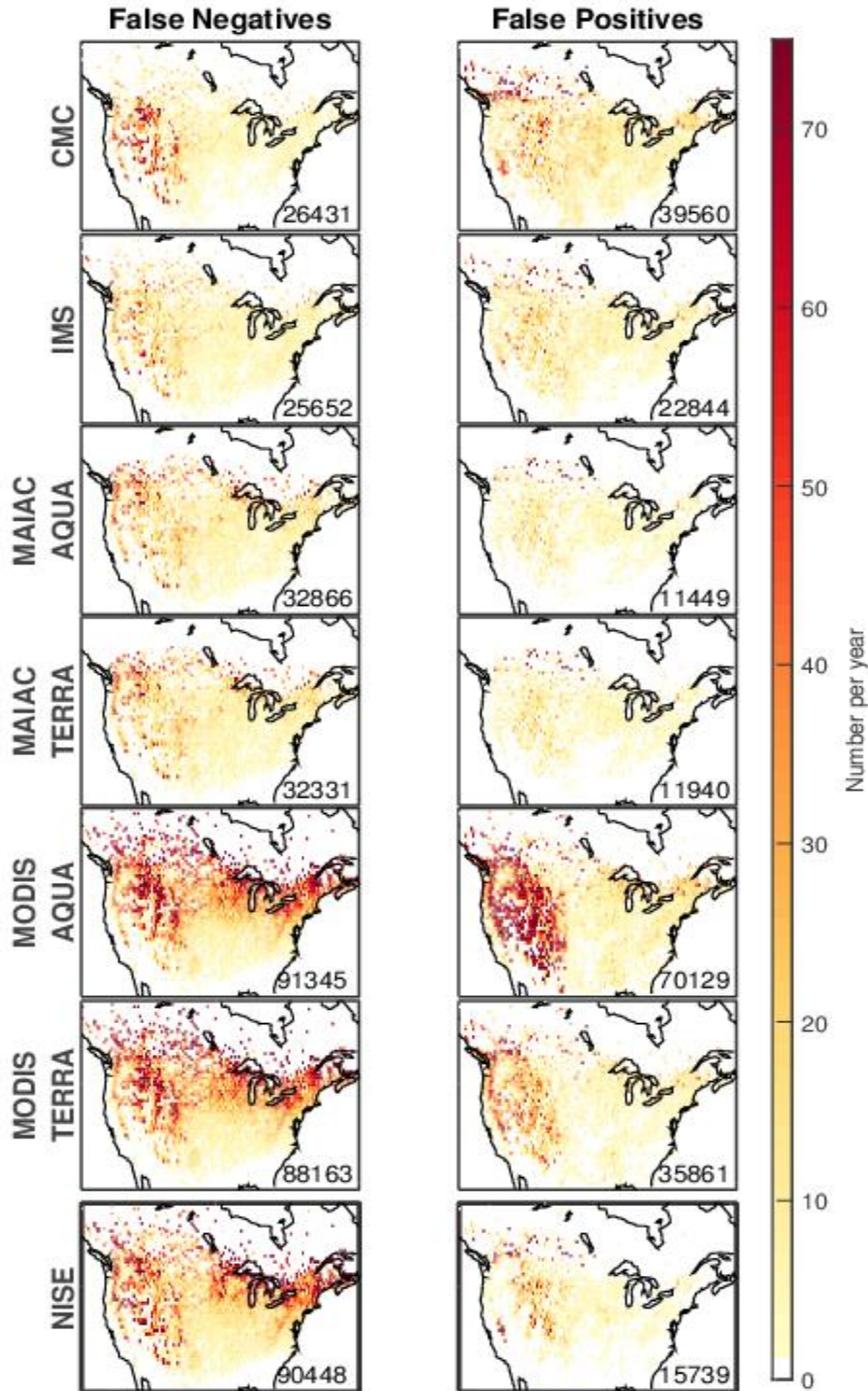
Figure 4: Number of false positive (FP) and false negative (FN) snow attributions by the snow
data sets in 2015. All data sets are evaluated at 4 km resolution. Total number of false snow
attributions inset. White space indicates that no ground stations are present.
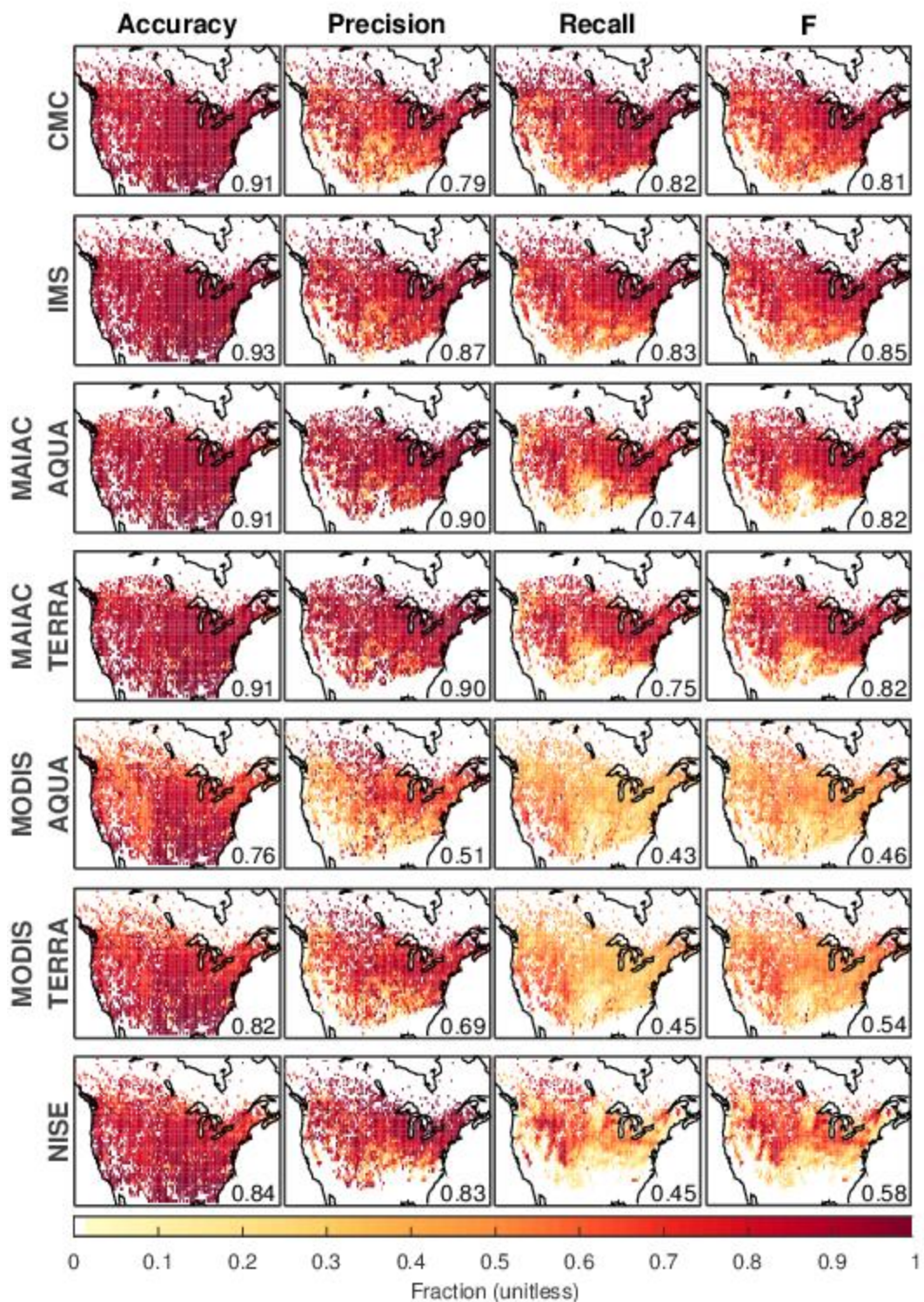
Figure 5: Statistical metrics to evaluate snow cover products. All data sets are gridded at 4 km resolution. White space indicates that no ground stations are present.
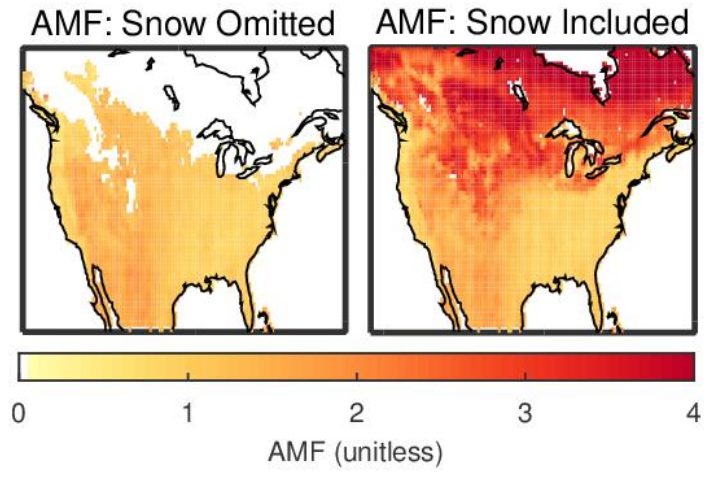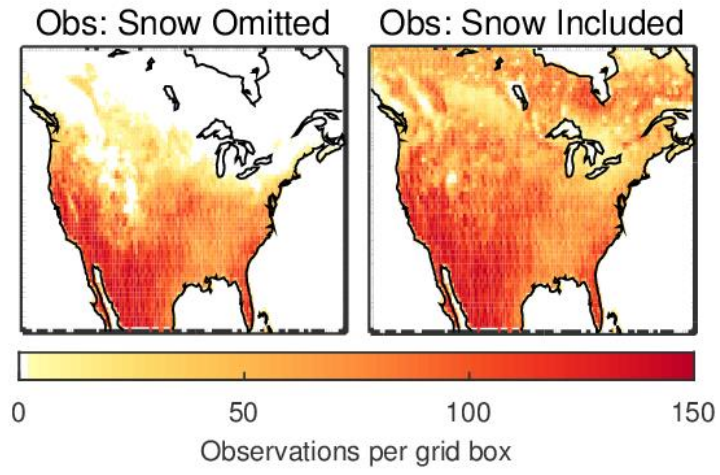
Figure 6: OMI observation frequency (top) and average AMFs (bottom) over North America in January using IMS to identify surface snow conditions. White space indicates a lack of observations.

577

	Accuracy	Precision	Recall	F
CMC	0.91	0.79	**0.83**	0.81
IMS	**0.93**	0.87	**0.83**	**0.85**
MAIAC AQUA	0.91	**0.90**	0.74	0.82
MAIAC TERRA	0.91	**0.90**	0.75	0.82
MODIS AQUA	0.76	0.51	0.43	0.46
MODIS TERRA	0.82	0.69	0.45	0.54
NISE	0.84	0.83	0.45	0.58

578 Table 1: Evaluation of daily snow extent data set performance for 2015. GHCN-D surface

579 observations are used as "truth". All products are regridded to a common 4 km resolution. The

580 highest value for each metric is shown in bold.

581 **Appendix**

Months	Data set	Accuracy	Precision	Recall	F
	CMC	0.84	0.84	0.89	0.86
	IMS	**0.88**	0.90	**0.88**	**0.89**
	MAIAC AQUA	0.84	**0.93**	0.80	0.86
DJF	MAIAC TERRA	0.84	0.92	0.80	0.86
	MODIS AQUA	0.58	0.84	0.34	0.48
	MODIS TERRA	0.60	0.88	0.37	0.52
	NISE	0.63	0.90	0.41	0.57
	CMC	0.90	0.63	0.57	0.59
	IMS	**0.93**	0.74	**0.67**	0.70
	MAIAC AQUA	**0.93**	**0.81**	0.62	**0.71**
MAM	MAIAC TERRA	**0.93**	**0.81**	0.63	**0.71**
	MODIS AQUA	0.86	0.43	0.39	0.41
	MODIS TERRA	0.89	0.62	0.40	0.49
	NISE	0.90	0.71	0.34	0.46
	CMC	0.91	0.73	**0.81**	0.76
	IMS	**0.92**	0.82	0.74	**0.78**
	MAIAC AQUA	0.91	**0.86**	0.60	0.71
SON	MAIAC TERRA	0.90	0.85	0.61	0.71
	MODIS AQUA	0.82	0.51	0.36	0.42
	MODIS TERRA	0.86	0.71	0.39	0.51
	NISE	0.85	0.85	0.25	0.39

582 Table A1: Evaluation of daily snow extent data set performance by season for 2015. GHCN-D

583 surface observations are used as "truth". All products are regridded to a common 4 km

584 resolution. The highest value for each metric/season is shown in bold.

585

586

	Resolution	Accuracy	Precision	Recall	F
CMC	25 km	0.92	0.81	0.81	0.81
IMS	4 km	**0.93**	0.87	**0.83**	**0.85**
MAIAC AQUA	1 km	0.91	**0.91**	0.71	0.80
MAIAC TERRA	1 km	0.91	0.90	0.71	0.80
MODIS AQUA	0.05°	0.77	0.50	0.30	0.37
MODIS TERRA	0.05°	0.81	0.65	0.32	0.43
NISE	25 km	0.85	0.87	0.37	0.51

587 Table A2: Evaluation of daily snow extent data set performance for 2015. GHCN-D surface

588 observations are used as "truth". The highest value for each metric is shown in bold.

589

	Accuracy	Precision	Recall	F
CMC	0.92	0.81	0.81	0.81
IMS	**0.93**	0.84	**0.85**	**0.84**
MAIAC AQUA	0.87	0.69	0.73	0.71
MAIAC TERRA	0.88	0.68	0.73	0.71
MODIS AQUA	0.78	0.50	0.41	0.45
MODIS TERRA	0.83	0.68	0.43	0.53
NISE	0.85	**0.87**	0.37	0.52

590 Table A3: Evaluation of daily snow extent data set performance for 2015. GHCN-D surface

591 observations are used as "truth". All products are regridded to a common 25 km resolution. The

592 highest value for each metric is shown in bold.